



Published in final edited form as:

ACS Nano. 2013 October 22; 7(10): 8715–8727. doi:10.1021/nn403080y.

Biological and Environmental Transformations of Copper-Based Nanomaterials

Zhongying Wang¹, Annette Von Dem Bussche³, Pranita K. Kabadi³, Agnes B. Kane^{3,4}, and Robert H. Hurt^{2,4,*}

¹Department of Chemistry, Brown University, Providence, Rhode Island 02912

²School of Engineering, Brown University, Providence, Rhode Island 02912

³Department of Pathology and Laboratory Medicine, Brown University, Providence, Rhode Island 02912

⁴Institute for Molecular and Nanoscale Innovation, Brown University, Providence, Rhode Island 02912

Abstract

Copper-based nanoparticles are an important class of materials with applications as catalysts, conductive inks, and antimicrobial agents. Environmental and safety issues are particularly important for copper-based nanomaterials because of their potential large-scale use and their high redox activity and toxicity reported from *in vitro* studies. Elemental nanocopper oxidizes readily upon atmospheric exposure during storage and use, so copper oxides are highly relevant phases to consider in studies of environmental and health impacts. Here we show that copper oxide nanoparticles undergo profound chemical transformations under conditions relevant to living systems and the natural environment. Copper oxide nanoparticle (CuO-NP) dissolution occurs at lysosomal pH (4–5), but not at neutral pH in pure water. Despite the near-neutral pH of cell culture medium, CuO-NPs undergo significant dissolution in media over time scales relevant to toxicity testing due to ligand-assisted ion release, in which amino acid complexation is an important contributor. Electron paramagnetic resonance (EPR) spectroscopy shows that dissolved copper in association with CuO-NPs are the primary redox-active species. CuO-NPs also undergo sulfidation by a dissolution-precipitation mechanism, and the new sulfide surfaces act as catalysts for sulfide oxidation. Copper sulfide NPs are found to be much less cytotoxic than CuO NPs, which is consistent with the very low solubility of CuS. Despite this low solubility of CuS, EPR studies show that sulfidated CuO continues to generate some ROS activity due to the release of free copper by H₂O₂ oxidation during the Fenton-chemistry-based EPR assay. While sulfidation can serve as a natural detoxification process for nanosilver and other chalcophile metals, our results suggest that sulfidation may not fully and permanently detoxify copper in biological or environmental compartments that contain reactive oxygen species.

*Address correspondence to Robert_Hurt@brown.edu.

Conflict of Interest: The authors declare no competing financial interest.

Supporting Information **Available:** Additional details about Visual MINTEQ 3.0 calculations, characterization of commercial CuO nanoparticles, time-dependent dissolution of CuO nanoparticles in PBS buffer (pH 7.4), the effects of various components in cell culture media on the dissolution of CuO in PBS buffer, hydroxyl radical induced by 0.032 ppm Cu²⁺ with 1 mM glutamine in PBS buffer after 20 min, 45 min, 95 min incubation, HRTEM image of sulfidated CuO nanoparticles showing the lattice fringes, sulfidation of CuO NPs and the catalytic ability of CuS, and viability of murine macrophages exposed to 5, 10, or 20 ppm of carbon black, CuO, and CuS NPs for 24 hours. This material is available free of charge *via* the Internet at <http://pubs.acs.org>.

Keywords

Human health; environment; nano-copper; toxicity; redox activity; phase transformations

Copper-based nanomaterials are used in a range of established and emerging technologies that include catalysts, printable electronics, magnetic storage, solar energy conversion, wood protection and antimicrobial products.¹⁻⁷ These uses will inevitably lead to human and environmental exposures that must be characterized and managed to ensure the safe development of copper-based nanotechnologies. In addition to engineered nanoparticles, copper also occurs as an “incidental” particle generated by chemo-mechanical polishing operations on copper-containing substrates in the semiconductor industry.⁸ Copper-containing materials are widely used as antimicrobials and in agriculture as fungicides, algaecide, and herbicides. Relevant copper forms include carbonates, hydroxides, various oxide phases, and the zero-valent metal, and dissolution to bioavailable ions is a commonly assumed mode of activity. In other application fields, the most technologically important copper-based materials are zero-valent metal nanoparticles (Cu-NPs) and oxide nanoparticles, Cu_xO-NP, with x=1 or 2. The potential for widespread exposure makes copper-based nanomaterials a high priority for risk characterization.

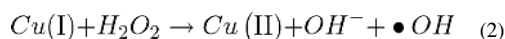
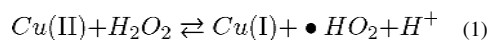
A second factor making nano-copper a high priority for study is its significant toxicity relative to other common nanomaterials.⁹⁻¹⁶ Karlsson *et al.*¹⁵ found that CuO nanoparticles were the most potent regarding DNA damage and cytotoxicity in a set of metal oxides and carbons studied in parallel. Fahmy *et al.*¹⁷ showed greater cytotoxicity of CuO nanoparticles in airway epithelial (HEp-2) cells relative to SiO₂ and Fe₂O₃ and demonstrated that oxidative stress was the cause of the cytotoxic effect. Studer *et al.*¹⁴ attributed the cytotoxicity of CuO to its relatively high solubility in biological media and the impacts of dissolved copper ions, as also reported by Zhang *et al.*⁹ There is a general consensus that toxicity in Cu/Cu_xO materials is due to oxidative pathways, but there is ongoing debate about the relative importance of ions and particle surfaces in primary ROS generation.¹⁸

It has become clear that nanomaterials can undergo chemical transformation in the environment or human body that profoundly influences their toxicity and risk.¹⁹⁻²⁴ This is especially important for metal-based nanomaterials, where the base metals themselves are indefinitely persistent, but can occur in different compounds or phases that greatly affect metal bioavailability. Nanosilver for example, is synthesized and sold in metallic form, but over its lifetime can undergo oxidative dissolution, colloidal aggregation, sulfidation, and reaction with selenium with corresponding large changes in silver bioavailability and toxicity.^{19, 22, 23, 25-29} ZnO nanoparticles have been reported to partially dissolve in environmental and biological media and exert toxicity through the liberated zinc ions,^{9, 30, 31} or to undergo sulfidation to the more stable ZnS.³²

Several studies have examined transformations in copper-based systems.^{10, 33} In comparison to silver, metallic copper NPs oxidize more readily, first forming a Cu(I) oxide shell around a zero-valent core, and eventually to Cu(II) oxide as a final product.¹⁰ Oxidation typically begins during fabrication and storage, so at the point of exposure or environmental release, an oxide or surface oxide is the most likely phase to come into contact with biological and environmental fluid phases.^{10, 34, 35} For this reason, and because the oxidation process has already been systematically studied,¹⁰ we chose to focus our study on the interactions of pre-existing copper oxide phases with biological and environmental systems.

There is significant evidence that dissolution is an important transformation in oxidized copper NPs.^{9, 10, 13, 14, 33} Though generally regarded as “insoluble” substances, copper and

copper oxides NPs appear to liberate sufficient amounts of soluble copper in relevant media to affect biological systems. Zhang *et al.*⁹ measured the extent of dissolution of CuO in biological media and attributed cytotoxicity of CuO to the soluble fraction rather than particle surface reactions. Studer *et al.*¹⁴ proposed a Trojan horse-type mechanism in which CuO nanoparticles penetrated the cell membrane followed by intracellular dissolution into redox active copper ions. Midander *et al.*³³ observed size-dependent ion release and toxicity when comparing nano- and micrometer-sized copper oxide particles. Free copper ions Cu^{x+} ($x=1,2$) are highly redox active species capable of producing hydroxyl radical by the Fenton-like reaction:^{36, 37}



so even small amounts of soluble copper can be biologically significant. Based on recent work on the dissolution in other NP systems, we hypothesize that pH, ionic strength, dissolved organic matter, and biomolecular ligands may play an important role in the toxicity of copper-based nanoparticles by influencing the total dissolved copper concentration.³⁸ This concentration, together with the relative redox activity of the ion and surface, should determine the origin of ROS generation and subsequent toxicity pathways in Cu-based nanomaterials, which are factors we hope to clarify in this study.

A final relevant transformation is reaction involving the earth-abundant element sulfur, which has been shown to be important for silver, zinc, and Cd nanomaterials³⁹ in both environmental^{32, 40-43} and biological settings.²² Copper ions are soft (Cu^+) or borderline (Cu^{2+}) Lewis acids with high affinity for sulfide ligand, and form a highly insoluble sulfide phase, which suggests that copper oxides may undergo sulfidation to produce a material with low copper bioavailability. The synthesis literature shows that hollow CuS nanostructures can be synthesized using Cu_2O as sacrificial template,^{44, 45} but information on the natural bio-environmental sulfidation pathways are limited. Sulfidation has been suggested as a natural detoxification process for metallic nanoparticles.^{40, 46, 47}

The present study investigates the transformations of copper oxide nanoparticles in biological and environmental media, and their implications for copper bioavailability, redox activity, and toxicity. The results are directly relevant to CuO-based technologies, and may provide qualitative insight into technologies based on metallic Cu or Cu(I) oxide materials that are capable of environmental oxidation to CuO or CuO outer corrosion films. We show that copper oxide undergoes acid-promoted dissolution, but also ligand-assisted dissolution in the presence of amino acids at neutral pH. Copper oxide also undergoes sulfidation to produce highly insoluble CuS nanoparticles. Surprisingly, sulfidation does not permanently suppress copper bioavailability and redox activity, because hydrogen peroxide at physiologically relevant concentrations oxidizes CuS and liberates free copper ions that partially restore redox activity in the form of OH \cdot detected here by EPR methods.³⁶

Results and Discussion

Comparative solubilities of oxide and sulfide phases

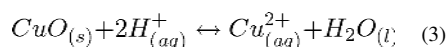
Ion-particle partitioning is a major determinant of the fate, transport, and toxicity of nanoparticles, and understanding dissolution behavior has become an important theme in environmental nanotechnology and nanotoxicology research.^{9, 19, 21, 30, 46, 48-50} Figure 1 shows the equilibrium solubilities of oxide and sulfide phases for several metals found in the

most common commercial nanomaterial types. Although based on bulk thermodynamic properties, this plot shows several trends that provide insight into reported nanomaterial behavior. First, the most soluble oxides are those of Ag, Ni, and Zn, and all three have been reported to be toxic through dissolution mechanisms.^{31, 51, 52} ZnO toxicity has been related to dissolution in several recent studies^{9, 30, 31} and NiO toxicity *in vitro* has been reported to correlate with the concentration of dissolved Ni²⁺ ion.⁵¹ Silver oxidizes slowly and is typically synthesized and sold as the zero-valent metal, but does dissolve upon use and disposal^{46, 49} through a mechanism that may pass through a Ag₂O surface intermediate.⁵³ Because the oxide has a relatively high solubility, the rate limiting step is typically the initial oxidation step.^{54, 55} Lower solubility oxides are titania, whose biological responses have not typically been related to dissolution, and copper, the subject of the present study.

Sulfide phases are typically much less soluble, and have been reported to form when nanosilver is exposed to the natural environment^{23, 24, 40-43, 47} or biological fluid phases,²² and to reduce the toxicity relative to the original zero-valent form.^{23, 40, 47, 56} Sulfidation has been proposed as a natural detoxification mechanism for nanosilver^{40, 41, 47} and potentially other chalcophile metals.^{57, 58} This is based on the fact that the equilibrium free metal in each of these sulfide systems is in the nanomolar range or below (Figure 1), which is well below typical threshold concentrations for biological effects. Copper(I) sulfide, CuS, is unique in its extremely low solubility (Figure 1), which led us to hypothesize that sulfidation would effectively detoxify nano-Cu or nano-CuO. We found here, however, that copper sulfides do form, but the redox activity of the product is not fully suppressed (*vide infra*).

Copper ion release in biological and environmental relevant media

Copper (II) oxide is described as insoluble in basic chemistry references, but at the ppm levels of interest in nanotoxicology and the environment it is sufficiently soluble for the released ions to be key determinants of toxicity.^{9, 13, 14} Based on Equation 3, we expect CuO ion release to be pH dependent, and this is confirmed in Figure 2A. Solubility at lysosomal pH (4-5) is significant, and can be close to complete at low particle loadings (Figure 2B), but at extracellular pH (7.4 in PBS buffer) is very low. The very low ion release at pH 7.4 was initially surprising since copper ions have been reported to be the primary source of toxicity in several *in vitro* studies.^{9, 13, 14} Calculations with Visual MINTEQ 3.0 at this pH confirm low values of dissolved copper ion (154 ppb) at equilibrium. These low values were further confirmed in time-resolved measurements (Supporting Information, Figure S2A), which gave copper concentrations about 20 ppb, which approached the detection limit of our inductively coupled plasma atomic emission spectroscopy (ICP-AES) technique.



To understand how Cu-ions exist in biological studies, we studied dissolution directly in two types of cell culture media (Figure 2C). We measure significant release in both media despite the high pH (7.4), suggesting dissolution is assisted by ligands, either thermodynamically by reducing the concentration of the free ion in equilibrium with the solid, and/or through kinetic effects at the particle surface. We tested a variety of single components found in cell culture media in an attempt to identify the primary types of ligands involved. Glucose and the buffering agent, HEPES, did not promote copper ion release, but FBS (fetal bovine serum) and glutamine did (Figure S2B). Glutamine and other amino acids have been reported to form a high-affinity complex with copper, and the overall stability constant is very high ($\log\beta_2$ of 11.6).⁶³ The removal of free ion shifts the ion-particle equilibrium and favors dissolution. The complex formation (stability) equilibrium constant, $K = [L-Cu^{2+}]/[Cu^{2+}][L]$, can be rearranged to give a dissolution enhancement factor:

$$[\text{total copper}] / [\text{free ion}] = ([L - \text{Cu}^{2+}] + [\text{Cu}^{2+}]) / [\text{Cu}^{2+}] = 1 + K[L] \quad (4)$$

which is $10^8 - 10^9$ when the concentration of ligands (*e.g.* glutamine) in cell culture media is in the mM range. We further investigated the effects of a larger series of amino acids (Figure 2D), which all promoted dissolution, but to differing degrees. We thought this may be due to involvement of the side chain in complex formation, but previous studies have reported that only the amino and carboxylate terminal groups were involved.⁶⁴ Indeed the Cu^{2+} complexes with glutamine and histidine do not have higher stability constants than other amino acids, which also suggests their higher activity is not thermodynamic in origin. In the search for an alternative explanation, ligands have been reported to promote the dissolution of iron oxide through formation of surface complexes that kinetically enhance the detachment.⁶⁵ The surface binding constant for CuO-histidine is reported to be higher than that for other amino acids,⁶⁶ and the ion concentrations in Figure 2A are well below estimated equilibrium values (see horizontal bars). Both of these facts suggest the different activities among the amino acids are kinetics differences associated with ligand-specific surface binding ability.

ROS production in Cu-NP systems

Several studies of nano-Cu or nano-CuO toxicity report ROS generation and oxidative stress as a mechanism.^{12, 16, 17} In copper-containing systems, ROS may be produced by heterogeneous reactions at the particle surfaces, or by dissolved copper, which can exhibit Fenton-like chemistry through the Cu(II)/Cu(I) redox couple.^{12, 67, 68} Resolving the relative particle-ion contributions is key to understanding the mechanism of nano-Cu toxicity and interpreting nanotoxicology data. Studies showing correlation between dissolved Cu and toxicity suggest the primary redox species are in solution,¹³ not on the surface, but direct evidence is needed. Here, we use EPR spin-trap techniques to quantify ROS production from particles, ions, and sulfidated products. We focus on the hydroxyl radical by using the spin trap DMPO, which is known to react with $\cdot\text{OH}$ to form an OH-DMPO adduct that exhibits a characteristic EPR peak quartet (see Fig. 3). Incubation of CuO NPs or copper ions with DMPO and peroxide in PBS buffer gives this characteristic EPR spectra, but with varying peak intensities as shown in Fig. 3. Each of the copper-containing solutions triggers Fenton chemistry and produces the OH-DMPO adduct. Comparing the data on particles and their clear filtrates (Figure 3A) indicates that most of the activity in the CuO NP cases is associated with the soluble fraction. Figure 2 predicts that this soluble fraction should be quite low under these conditions (< 100 ppb), and indeed the “ion-only” experiments in Fig. 3B show similar peak heights for 6-100 ppb free copper. Even at this limited degree of dissolution (neutral pH with no added ligands), the main source of ROS is the trace concentration of free copper ion.

We were interested in whether the ligands that promote Cu dissolution also affect redox activity in solution. Previous studies have shown that complex formation can reduce the catalytic ability of Cu ions in peroxide reduction to $\cdot\text{OH}$.⁶⁹ Figure 4 shows a strong attenuation of the $\cdot\text{OH}$ signal when simple PBS buffer (Figure 3) is replaced by cell culture medium (Figure 4A). Some redox activity remains in media (the OH-DMPO quartet is clearly visible), and is primarily associated with the soluble fraction, since the particles and their clear filtrates give similar peak heights (Figure 4A). The redox behavior is quite low in the presence of 1 mM glutamine (Figure 4B), which is a high affinity ligand ($\log\beta_2$ of 11.6) and strong promoter of dissolution.

The catalytic ROS production by Cu is significantly reduced in the media containing glutamine, but the complexed Cu can still catalyze the reaction though in a much slower manner (Figure S3) Overall, the data in Figures 2-4 suggest that complex biological media

will promote copper dissolution but then partially suppress the redox activity of the resulting soluble species. It is doubtful that simple assays for dissolution and redox activity in water or simple buffers will have predictive value for the toxicity of copper-containing NPs.

Copper oxide sulfidation

Recent research has shown that nanoparticles based on silver, zinc and cadmium undergo reactions with reduced sulfur species (and in some cases selenium species)²² in the environment and the human body to produce low-solubility metal sulfide (or selenide) phases. These transformations are expected to have profound effects on transport, bioavailability, toxicity and risk.^{22-24, 32, 40, 46, 47, 57, 70} Here we studied the reaction of CuO-NPs with soluble sulfide (main species is HS⁻) as a function of time and CuO:sulfide stoichiometric ratios. Figure 5 shows conversion of CuO NPs to sulfide phases within one day with the extent of conversion depending on the starting CuO:bisulfide molar ratio. At high sulfide (CuO:bisulfide = 1:5) the conversion is essentially complete as the XRD spectra lose all characteristic peaks for crystalline CuO and match quite well with Cu(I)S (covellite) reference spectra (Figure 5A). Though the formation of any Cu₂S phase was not observed, absence of a crystalline Cu₂S phase under these conditions may indicate a slow phase transition that prevents the crystalline phase from being observed over our time scales.⁷¹ The morphologies of the sulfidated samples show a number of particles substantially smaller than the original CuO particles, and at least some of them in a crystalline state, indicated by HRTEM fringes (Figure 5B, Figure S4). The theoretical amount of bisulfide needed to stoichiometrically convert CuO to CuS is only at the ratio 1:1, but the data in Figure 5 only achieve complete sulfidation at the ratio 5:1, so sulfidation is either limited by kinetics, or there are competing reactions for bisulfide (*vide infra*).

We carried out additional experiments to understand the sulfidation mechanism and reaction stoichiometry. The presence of small particles surrounding a central core suggests a dissolution-precipitation mechanism rather than a direct solid-state exchange reaction. Recent research has reported dissolution-precipitation mechanism for the sulfidation of ZnO NPs³² with similar morphologies in the sulfidation products.

To better understand sulfidation pathways, we interrupted the sulfidation process and examined the soluble products or clusters (after half hour incubation) that passed through a 200 nm syringe filter.⁷² Figure 6B shows UV-vis spectra of this filtrate after aging for up to 3 hours, which shows an absorption feature that starts to appear around 600 nm that likely belongs to CuS.⁷³ The aged filtrate was washed three times with water and then concentrated for DLS analysis (Figure 6C), which shows 10 nm mean particle size. These are much smaller than the starting CuO NPs (50 nm) suggesting they are secondary particles/clusters formed by dissolution-precipitation. XRD analysis identifies them as CuS (Figure 6D). We also investigated the filtrate of the solution after 3 hour incubation and did not observe the characteristic CuS peak, which suggests these ultrafine CuS clusters have grown or else attached to larger particles.⁴⁰ As a control we incubated CuO NPs in NaOH at the same pH (9.3) as the sulfide solutions (but without sulfide) and performed the ultrafiltration, but did not see particles/clusters in the filtrate. The filtrate from this control was treated with sulfide and the product investigated with UV-vis, but no characteristic CuS peak was observed. In another separate experiment, the filtrate was digested with nitric acid and prepared for ICP-AES analysis to determine the copper concentration. No detectable copper was found in the filtrate by ICP-AES. Together these data indicate that CuO NPs undergo rapid sulfidation and the mechanism involves dissolution-precipitation. However, the detection of secondary CuS nanoparticles does not exclude the possibility of some direct solid-phase conversion. It is interesting that this can even occur at high pH (9.3) where CuO dissolution is extremely limited. Bisulfide is a high-affinity ligand for ionic copper, and the

data indicate that it promotes copper dissolution from CuO NPs at the same time it forms the insoluble CuS phases as secondary particles in the immediate vicinity of the mobilization sites. The dual role of bisulfide as dissolution promoter and precipitating agent explain the essential behavior in Figure 6.

Properties of CuS - catalysis of sulfide oxidation

The data in Figure 5 show that a great excess of bisulfide is needed to fully convert CuO NPs to CuS. While this could indicate kinetic limitations for this reaction, we instead have evidence that it is due to bisulfide consumption by oxygen that is catalyzed by the same CuS that is produced as the sulfidation product. In time-resolved studies we observed a rapid depletion of bisulfide upon addition of copper oxide nanoparticles (Figure S5 A), even if the bisulfide concentration was 5 times greater than the Cu on a molar basis. This cannot be explained by CuS precipitation stoichiometry, and instead must indicate either superstoichiometric sulfide phases or catalytic loss of bisulfide by oxidation. The XRD results show CuS as a main product, so bisulfide oxidation seemed more likely. To test this hypothesis, we added copper chloride (the concentration is 0.1, 1 or 2 mM, respectively) to existing excess bisulfide solutions and saw rapid drops in dissolved oxygen concentration (Figure 7A). The O₂ depletion rate increased with increasing Cu²⁺ addition. Copper ion has been shown to catalyze the oxidation of bisulfide in the presence of oxygen,⁷⁴ and the reduction of Cu (II) to Cu(I) has been observed on the surface of CuO when incubated in bisulfide solutions.⁷⁵ However, in our experiments it was still not clear whether dissolved copper ions or CuO nanoparticles were the active catalyst. To investigate this, the catalytic ability of CuO nanoparticles was compared with that of equimolar Cu ion in excess bisulfide solution and the depletion of bisulfide was also monitored at the same time. Figure S5 (B) shows the depletion of bisulfide is much faster in the presence of free Cu ion than the presence of CuO nanoparticles. Therefore, catalytic ability of CuO nanoparticles in bisulfide oxidation is not significant. Further, the oxygen concentrations were unchanged if copper ion was added in equimolar amounts to HS⁻ to make stoichiometric CuS, which indicated copper ions readily reacted with bisulfide before catalyzing the oxidation of bisulfide. Overall it is clear that CuS is the catalytic phase for bisulfide oxidation.⁷⁶ Comparison experiments indicated both the soluble CuS clusters and CuS particles contribute to the catalytic oxidation of bisulfide in the presence of oxygen. (Figure S5 C)

Implications for Cu-NP Toxicity

The environmental transformation of a nanomaterial immediately raises questions about the behavior and toxicity of the transformed product(s), which may represent a greater or less risk than the original material. Metal sulfidation is often regarded as a passivation or detoxification process^{57, 58} due to the very low equilibrium solubilities and thus metal bioavailabilities of the sulfide phases (Figure 1).

We were also surprised, however to observe that CuS NPs and sulfidated CuO-NPs continued to show redox activity in our EPR Fenton assay (Figure S5C, Figure 7C). These CuS NPs were made by Cu²⁺/S²⁻ precipitation processes and the excess ions were removed by water washing prior to the ROS assay. Here again soluble species were the source of the redox activity, as evidenced by comparing the particle-induced ROS to that of filtrate, which were similar (Figure 7C). Although CuS is highly insoluble, the ROS assay uses H₂O₂ as a reactant, and we hypothesized that the soluble, redox-active species were copper ions produced by peroxide oxidation of CuS. Sulfide can be oxidized, and the conversion to oxidized sulfur species may destabilize copper in the CuS lattice and lead to ion release and solution-based Fenton activity.

To pursue this hypothesis, we studied copper mobilization from CuS NPs and a series of partially sulfidated CuO NPs (Figure 7D). Partial sulfidation has almost no effect on the rate of copper release from the CuO NPs undergoing transformation (bisulfide:CuO ratios from 1:5 up to 1:1). It is clear that partial sulfidation does not passivate CuO surfaces, which is consistent with the dissolution-precipitation mechanism that produces distinct secondary particles rather than protective coatings. Only at bisulfide:CuO ratios above 2:1 do we begin to see reductions in soluble copper release. The model CuS nanoparticles formed from Cu^{2+} and S^{2-} showed very low copper ion release, as expected, but addition of H_2O_2 at the 60 hr time point caused significant release (Figure 7D, green circles). In fact, EPR results suggest much more copper ions released from CuS than CuO when both were exposed to H_2O_2 at the same pH. These data provide support for CuS oxidation by H_2O_2 as the source of the redox activity seen in the EPR spectra of Figure 7C. The combined results suggest that sulfidation of Cu NPs or CuO NPs can reduce copper metal bioavailability, but only if the sulfidation is extensive and progresses to near stoichiometric completion, and oxidation with re-release of soluble copper may prevent CuS from being a fully nontoxic end state for copper-containing nanomaterials in the environment. Others have reported that nanoscale Cu and Zn sulfides are not fully stable and can transform into other species under aerobic conditions.^{77, 78}

Finally, we were interested in the biological implications of copper material transformations, and the effects of sulfidation on toxicity in particular. Previous studies showed that copper nanoparticles are internalized by target cells and release soluble ions more rapidly than micron-sized particles at the acidic pH in lysosomes as predicted by the “Trojan-horse mechanism” for metallic nanoparticle toxicity.^{33, 79} Here, uptake and toxicity of CuO and CuS NPs were assessed using a murine macrophage cell line in cell culture in comparison with carbon black nanoparticles as a nontoxic particle control. Following exposure to test and control particles for 3 hours, well-dispersed particles were visualized in the cytoplasm of target cells (Fig. 8A). Cell viability was assessed after 24 hours using a combination of brightfield (Figure 8B) and fluorescence (Figure 8C) microscopy. Only CuO NPs induced cell death and detachment after 24 hours. Intracellular mobilization of Cu ions induces redox cycling resulting in generation of ROS, induction of oxidative stress, and cell death.⁸⁰ Delivery of CuO or CuS NPs, triggered generation of higher levels of H_2O_2 in murine macrophages after 20 min compared to untreated cells or cells exposed to carbon black NPs. (Figure 9A). Over the same range of doses, CuO NPs induced significantly higher toxicity than CuS NPs after 24 hours (Figure S7) and 48 hours (Figure 9B), consistent with the lower Cu bioavailability in CuS.

Conclusions

Copper-containing nanomaterials are a particularly complex case for EHS studies, since they undergo oxidation, dissolution, sulfidation, and further oxidation of the sulfide phases over the time scales relevant for human health and environmental impacts. Figure 10 summarizes the main transformation and redox pathways observed for CuO NPs in this study. CuO NPs or oxide films on metallic Cu-NPs dissolve at low pH, or at neutral pH in the presence of ligands in biological environments, including those containing amine functional groups. The redox activity in copper NP systems appears to be associated with the soluble fraction and is mitigated but not eliminated by ligand binding in solution. CuO NPs undergo sulfidation through a dissolution/precipitation mechanism to produce complex secondary aggregates of CuS NPs. These CuS NPs are active catalysts for bisulfide oxidation. Sulfidation reduces Cu solubility, redox activity, and cytotoxicity but may not necessarily fully and permanently detoxify copper, since CuS can be oxidized in environments containing H_2O_2 to produce free copper that continues to cycle in solution producing hydroxyl radicals through Fenton-like chemistry. The results are directly relevant for CuO NPs, and may also be qualitatively

relevant for elemental nano-copper whose surfaces consist of oxide phases following environmental exposure.

Materials and Methods

CuO NPs agent were purchased from Aldrich and used as received. The CuO nanoparticles were synthesized using the molten salt synthesis method according to manufacturer and some organic matter was observed on the surface according to FT-IR (Figure S1B). Phosphate buffered saline (PBS buffer, 10 \times) was obtained from Fisher Scientific (MA, USA) and diluted with DI (deionized) water before use. The particles were characterized for size (mean 50 nm determined by TEM), surface charge in PBS buffer (zeta potential -25 mV), size distribution in PBS buffer and crystalline phase (tenorite). (Supporting Information, Figure S1) The increased size of particles in PBS buffer indicated the aggregation of CuO nanoparticles.

CuO dissolution experiments

CuO-NPs (200 ppm) were incubated in biological or environment relevant media that included acetate buffers (50 mM, pH 4, 5 and 6), PBS buffer (1 \times concentration, pH 7.4) and borate buffers (50mM, pH 8 and 9) for pH control. Acetate buffer (pH 4.9) was used as lysosome-mimic, and DMEM and RPMI cell culture media were studied supplemented with 10% FBS. The use of simulant fluids in environmental and biological studies has many limitations, but does provide well defined environments for studying the chemical transformations of materials.⁸¹ Nanoparticles were dispersed by 15 min sonication in 5 ml of the solutions. After incubating for a pre-defined time period, the samples were centrifuged by centrifugal ultrafiltration (Amicon Ultra-4 3k) for 30 min at 4000 rpm to remove the solids, and the supernatant was separated for determination of Cu concentration by ICP-AES. All ion release experiments were conducted at room temperature (20 °C) unless noted. The ability of centrifugal ultrafiltration to remove the nanoparticles has been proved by previous reference.⁴⁹ Our control experiments show ultrafiltration can effectively remove CuO nanoparticles and the Cu ions retention by the ultrafiltration filters can be neglected. (Figure S6) Therefore, solubility is defined as free metal ions and its complex, which is almost the same as all forms of metal that pass through the unltrafiltration filters in our case.

Electron paramagnetic resonance ROS assay

The ability of CuO-NPs and/or associated soluble species to generate hydroxyl radical in the presence of H₂O₂ were quantified using \times (9.8 GHz)-band EPR measurements at room temperature using an EMX-plus CW spectrometer (Bruker Biospin) and the spin-trap DMPO (Dojindo Molecular Technologies, Inc). In a typical experiment, 2 or 20 ppm CuO-NPs were incubated with 100 mM DMPO, 1 mM H₂O₂ in PBS buffer (pH 7.4) for 20 min, and the reaction was initiated by addition of H₂O₂. Then the aqueous solution was drawn into 50 μ L capillary (Cat No. 53432-783, VWR), and the capillary was inserted into a quartz EPR capillary tube (4 mm OD \times 250 mm L \times 0.5 mm wall, Wilmad LabGlass, Buena, NJ). The data acquisition parameters were set as follows: Center Field, 3508.75 G; sweep width, 100 G; sweep time, 30 s; modulation amplitude, 1G; number of scans, 10; microwave power, 2 mW; conversion time, 30 ms; time constant, 81.92 ms. Though EPR cannot quantitatively measure the radical produced due to decomposition of DMPO-OH adduct, it can give a relative ROS intensity by comparing the peak height if the incubation time and instrument parameters are constant.

Sulfide and dissolved oxygen (DO) depletion measurements

The sulfidation of CuO NPs were studied by tracking sulfide depletion using the method of Liu *et al.*⁴¹ Soluble sulfide concentration was measured with a sulfide-ion-selective

electrode following removal of solids by centrifugal ultrafiltration (Amicon Ultra-4 3k). In a typical experiment, 1 mg CuO-NP powder was added to 4.5 mL DI water, followed with sonication for 15 min to disperse the aggregates, and then 0.5 mL of 125 mM Na₂S solution was added to initiate the reaction at a starting sulfide concentration of 12.5 mM. The pH of 12.5 mM Na₂S solution is around 9.3, where the main soluble sulfide species is bisulfide (HS⁻). After rotating the mixture for a pre-determined time, the bisulfide solution was separated by centrifugal ultrafiltration and the sulfide antioxidant buffer (ASOB, Orion 941609 Thermo Scientific) was added to prevent bisulfide oxidation and volatilization before analysis. Bisulfide concentration in the filtrate was measured with sulfide-ISE (Orion 9616BNWP Silver/Sulfide combination electrode, Thermo Scientific) at room temperature. DO levels were monitored *in situ* during incubation of either copper ions or CuO NPs in bisulfide solutions in a closed amber glass bottle under magnetic stirring using a DO probe (Orion 083010MD, Thermo Scientific) at 3 s sampling frequency.

Cell toxicity studies

An immortalized murine macrophage cell line, J774.A1 (ATCC number TIB-67) was used as a target cell for assessment of uptake, H₂O₂ generation, and toxicity of CuO and CuS NPs. Carbon black (M120, Cabot) with a primary particle diameter ~ 75 nm was used as a nontoxic reference particle. Test particles were dispersed in RPMI 1640 medium containing 1% FBS at a concentration of 250 ppm and sonicated at 100W in a Branson 2510 sonicating water bath for 60 min prior to dilution at final concentrations of 5-20 ppm in cell culture medium. Murine macrophages were cultured in RPMI 1640 medium (Invitrogen 11875) containing 10% FBS, 2 mM glutamine, 1 mM sodium pyruvate, and 500 ul penicillin-streptomycin in ultralow attachment culture dishes (Corning 3262) at 37°C in air with 5% CO₂. For microscopy, cells were plated on glass coverslips in 12 well plates (Coster, 22 mm in diameter) at 70% confluence and allowed to attach for 3 hours, then exposed to test particles for 3-24 hours. To visualize uptake of test particles, cells were rinsed and stained with 4',6-diamidino-2-phenylindole (DAPI) and visualized under brightfield and fluorescence illumination using a spinning disk Olympus confocal inverted microscope (Model 1x81). To assess viability, cells were visualized using brightfield imaging to assess morphology and cell detachment, and confirmed by staining with 1:1000 Syto 10/ethidium homodimer (Invitrogen) for 5 min. Viable (green fluorescence) and dead cells (red fluorescence) were imaged using a spinning disk Olympus confocal inverted microscope equipment with fluorescence filters. Cell viability using DNA content as a surrogate for cell number was quantitated using a fluorescence assay (Pico Green, Invitrogen) that quantitatively binds to DNA according to the manufacturer's instructions. For quantitation of H₂O₂ generation, murine macrophages were seeded in RPMI growth medium at 75,000 cells per well in a black clear bottom 96-well plate (Costar 3603). Cells were allowed to equilibrate overnight at 37 °C, after which growth medium was aspirated and subsequently replaced with 200 ul of medium per well containing 50 uM Amplex Red reagent (Invitrogen A1222), 2ul of 10 U/ml horse radish peroxidase (Invitrogen 012001), and 2.5, 5, and 10 ppm of test particles.⁸² Continuous fluorescence measurements were obtained using a spectrophotometer with an excitation of 566 nm and an emission of 587 nm. Data were acquired every 5 minutes and reported after 20 min of exposure to test particles. Statistical significance was determined using an unpaired *t*-test to compare differences between the means (\pm SD) of untreated and treated cultures in triplicate. A *p* value of <0.05 was considered to be statistically significant.

Product characterization

UV-vis spectra of sulfidated CuO NP samples were recorded on a V-630 spectrophotometer (Jasco, MD) over the range 400 to 800 nm. The sizes of secondary CuS particles (formed by dissolution and precipitation) were monitored using dynamic light scattering (DLS) with a

Zetasizer Nano ZS system (Malvern Instruments). The morphologies of the sulfidated CuO NPs were observed in high-resolution transmission electron microscopy (HRTEM) on a JEOL JEM-2010. The samples were prepared by placing one drop of purified sample solution on carbon-coated copper grids, followed by drying at room temperature overnight. The compositions and phases of sulfidated CuO samples were identified by X-ray diffraction spectrometry (XRD) on a Bruker AXS D8 Advance instrument with Cu K α radiation ($\lambda=1.5418\text{\AA}$). The XRD samples were prepared by adding purified and concentrated sulfidated CuO nanoparticles suspension onto a glass slide, followed by overnight drying.

Supplementary Material

Refer to Web version on PubMed Central for supplementary material.

Acknowledgments

This work was supported by the National Science Foundation (grant ECCS-1057547), the Superfund Research Program of the National Institute of Environmental Health Sciences (P42 ES013660) and a Training Grant from the National Institute of Environmental Health Sciences (T32 ES007272). The authors acknowledge discussions and technical assistance from Dr. Jingyu Liu, Joseph Orchardo, and Anthony McCormick.

References

1. Evans P, Matsunaga H, Kiguchi M. Large-Scale Application of Nanotechnology for Wood Protection. *Nat Nano*. 2008; 3:577–577.
2. Wu Y, Wadia C, Ma W, Sadler B, Alivisatos AP. Synthesis and Photovoltaic Application of Copper(I) Sulfide Nanocrystals. *Nano Lett*. 2008; 8:2551–2555. [PubMed: 18651779]
3. Youngil L, Jun-rak C, Kwi Jong L, Nathan ES, Donghoon K. Large-Scale Synthesis of Copper Nanoparticles by Chemically Controlled Reduction for Applications of Inkjet-Printed Electronics. *Nanotechnology*. 2008; 19:415604. [PubMed: 21832649]
4. Ren G, Hu D, Cheng EWC, Vargas-Reus MA, Reip P, Allaker RP. Characterisation of Copper Oxide Nanoparticles for Antimicrobial Applications. *Int J Antimicrob Agents*. 2009; 33:587–590. [PubMed: 19195845]
5. Pandey A, Brovelli S, Viswanatha R, Li L, Pietryga JM, Klimov VI, Crooker SA. Long-Lived Photoinduced Magnetization in Copper-Doped ZnSe-CdSe Core-Shell Nanocrystals. *Nat Nano*. 2012; 7:792–797.
6. Maithreepala RA, Doong Ra. Reductive Dechlorination of Carbon Tetrachloride in Aqueous Solutions Containing Ferrous and Copper Ions. *Environ Sci Technol*. 2004; 38:6676–6684. [PubMed: 15669327]
7. Doong, Ra; Chang, Sm; Tsai, Cw. Enhanced Photoactivity of Cu-Deposited Titanate Nanotubes for Removal of Bisphenol A. *Appl Catal, B*. 2013; 129:48–55.
8. Huang HL, Wang HP, Wei GT, Sun IW, Huang JF, Yang YW. Extraction of Nanosize Copper Pollutants with an Ionic Liquid. *Environ Sci Technol*. 2006; 40:4761–4764. [PubMed: 16913135]
9. Zhang H, Ji Z, Xia T, Meng H, Low-Kam C, Liu R, Pokhrel S, Lin S, Wang X, Liao YP, et al. Use of Metal Oxide Nanoparticle Band Gap to Develop a Predictive Paradigm for Oxidative Stress and Acute Pulmonary Inflammation. *ACS Nano*. 2012; 6:4349–4368. [PubMed: 22502734]
10. Mudunkotuwa IA, Pettibone JM, Grassian VH. Environmental Implications of Nanoparticle Aging in the Processing and Fate of Copper-Based Nanomaterials. *Environ Sci Technol*. 2012; 46:7001–7010. [PubMed: 22280489]
11. Li Y, Zhang W, Niu J, Chen Y. Mechanism of Photogenerated Reactive Oxygen Species and Correlation with the Antibacterial Properties of Engineered Metal-Oxide Nanoparticles. *ACS Nano*. 2012; 6:5164–5173. [PubMed: 22587225]
12. Applerot G, Lellouche J, Lipovsky A, Nitzan Y, Lubart R, Gedanken A, Banin E. Understanding the Antibacterial Mechanism of CuO Nanoparticles: Revealing the Route of Induced Oxidative Stress. *Small*. 2012; 8:3326–3337. [PubMed: 22888058]

13. Gunawan C, Teoh WY, Marquis CP, Amal R. Cytotoxic Origin of Copper(II) Oxide Nanoparticles: Comparative Studies with Micron-Sized Particles, Leachate, and Metal Salts. *ACS Nano*. 2011; 5:7214–7225. [PubMed: 21812479]
14. Studer AM, Limbach LK, Van Duc L, Krumeich F, Athanassiou EK, Gerber LC, Moch H, Stark WJ. Nanoparticle Cytotoxicity Depends on Intracellular Solubility: Comparison of Stabilized Copper Metal and Degradable Copper Oxide Nanoparticles. *Toxicol Lett*. 2010; 197:169–174. [PubMed: 20621582]
15. Karlsson HL, Cronholm P, Gustafsson J, Moller L. Copper Oxide Nanoparticles are Highly Toxic: A Comparison between Metal Oxide Nanoparticles and Carbon Nanotubes. *Chem Res Toxicol*. 2008; 21:1726–1732. [PubMed: 18710264]
16. Ahamed M, Siddiqui MA, Akhtar MJ, Ahmad I, Pant AB, Alhadlaq HA. Genotoxic Potential of Copper Oxide Nanoparticles in Human Lung Epithelial Cells. *Biochem Biophys Res Commun*. 2010; 396:578–583. [PubMed: 20447378]
17. Fahmy B, Cormier SA. Copper Oxide Nanoparticles Induce Oxidative Stress and Cytotoxicity in Airway Epithelial Cells. *Toxicol in Vitro*. 2009; 23:1365–1371. [PubMed: 19699289]
18. Jo HJ, Choi JW, Lee SH, Hong SW. Acute Toxicity of Ag and CuO Nanoparticle Suspensions against *Daphnia Magna*: The Importance of their Dissolved Fraction Varying with Preparation Methods. *J Hazard Mater*. 2012; 227–228:301–308.
19. Lowry GV, Gregory KB, Apte SC, Lead JR. Transformations of Nanomaterials in the Environment. *Environ Sci Technol*. 2012; 46:6893–6899. [PubMed: 22582927]
20. Borm P, Klaessig FC, Landry TD, Moudgil B, Pauluhn J, Thomas K, Trottier R, Wood S. Research Strategies for Safety Evaluation of Nanomaterials, Part V: Role of Dissolution in Biological Fate and Effects of Nanoscale Particles. *Toxicol Sci*. 2006; 90:23–32. [PubMed: 16396841]
21. Reidy B, Haase A, Luch A, Dawson K, Lynch I. Mechanisms of Silver Nanoparticle Release, Transformation and Toxicity: A Critical Review of Current Knowledge and Recommendations for Future Studies and Applications. *Materials*. 2013; 6:2295–2350.
22. Liu J, Wang Z, Liu FD, Kane AB, Hurt RH. Chemical Transformations of Nanosilver in Biological Environments. *ACS Nano*. 2012; 6:9887–9899. [PubMed: 23046098]
23. Levard C, Hotze EM, Lowry GV, Brown GE. Environmental transformations of Silver Nanoparticles: Impact on Stability and Toxicity. *Environ Sci Technol*. 2012; 46:6900–6914. [PubMed: 22339502]
24. Lowry GV, Espinasse BP, Badireddy AR, Richardson CJ, Reinsch BC, Bryant LD, Bone AJ, Deonarine A, Chae S, Therezien M, et al. Long-Term Transformation and Fate of Manufactured Ag Nanoparticles in a Simulated Large Scale Freshwater Emergent Wetland. *Environ Sci Technol*. 2012; 46:7027–7036. [PubMed: 22463850]
25. Kent RD, Vikesland PJ. Controlled Evaluation of Silver Nanoparticle Dissolution Using Atomic Force Microscopy. *Environ Sci Technol*. 2011; 46:6977–6984. [PubMed: 22191460]
26. Kennedy AJ, Hull MS, Bednar AJ, Goss JD, Gunter JC, Bouldin JL, Vikesland PJ, Steevens JA. Fractionating Nanosilver: Importance for Determining Toxicity to Aquatic Test Organisms. *Environ Sci Technol*. 2010; 44:9571–9577. [PubMed: 21082828]
27. Stebounova L, Guio E, Grassian V. Silver Nanoparticles in Simulated Biological Media: A Study of Aggregation, Sedimentation, and Dissolution. *J Nanopart Res*. 2011; 13:233–244.
28. Sotiriou GA, Pratsinis SE. Antibacterial Activity of Nanosilver Ions and Particles. *Environ Sci Technol*. 2010; 44:5649–5654. [PubMed: 20583805]
29. Lorenz C, Windler L, von Goetz N, Lehmann RP, Schuppler M, Hungerbühler K, Heuberger M, Nowack B. Characterization of Silver Release from Commercially Available Functional (Nano)Textiles. *Chemosphere*. 2012; 89:817–824. [PubMed: 22677521]
30. Xia T, Zhao Y, Sager T, George S, Pokhrel S, Li N, Schoenfeld D, Meng H, Lin S, Wang X, et al. Decreased Dissolution of ZnO by Iron Doping Yields Nanoparticles with Reduced Toxicity in the Rodent Lung and Zebrafish Embryos. *ACS Nano*. 2011; 5:1223–1235. [PubMed: 21250651]
31. Franklin NM, Rogers NJ, Apte SC, Batley GE, Gadd GE, Casey PS. Comparative Toxicity of Nanoparticulate ZnO, Bulk ZnO, and ZnCl₂ to a Freshwater Microalga (*Pseudokirchneriella Subcapitata*): The Importance of Particle Solubility. *Environ Sci Technol*. 2007; 41:8484–8490. [PubMed: 18200883]

32. Ma R, Levard C, Michel FM, Brown GE, Lowry GV. Sulfidation Mechanism for Zinc Oxide Nanoparticles and the Effect of Sulfidation on their Solubility. *Environ Sci Technol.* 2013; 47:2527–2534. [PubMed: 23425191]
33. Midander K, Cronholm P, Karlsson HL, Elihn K, Möller L, Leygraf C, Wallinder IO. Surface Characteristics, Copper Release, and Toxicity of Nano- and Micrometer-Sized Copper and Copper(II) Oxide Particles: A Cross-Disciplinary Study. *Small.* 2009; 5:389–399. [PubMed: 19148889]
34. Pettibone JM, Adamcakova-Dodd A, Thorne PS, O'Shaughnessy PT, Weydert JA, Grassian VH. Inflammatory Response of Mice Following Inhalation Exposure to Iron and Copper Nanoparticles. *Nanotoxicology.* 2008; 2:189–204.
35. Sotiriou GA, Meyer A, Knijnenburg JTN, Panke S, Pratsinis SE. Quantifying the Origin of Released Ag⁺ Ions from Nanosilver. *Langmuir.* 2012; 28:15929–15936. [PubMed: 23072572]
36. Yamamoto K, Kawanishi S. Hydroxyl Free Radical is Not the Main Active Species in Site-Specific DNA Damage Induced by Copper (II) Ion and Hydrogen Peroxide. *J Biol Chem.* 1989; 264:15435–40. [PubMed: 2549063]
37. Drouin R, Rodriguez H, Gao SW, Gebreyes Z, O'Connor TR, Holmquist GP, Akman SA. Cupric Ion/Ascorbate/Hydrogen Peroxide-Induced DNA Damage: DNA-Bound Copper Ion Primarily Induces Base Modifications. *Free Radical Biol Med.* 1996; 21:261–273. [PubMed: 8855437]
38. Erickson RJ, Benoit DA, Mattson VR, Leonard EN, Nelson HP. The Effects of Water Chemistry on the Toxicity of Copper to Fathead Minnows. *Environ Toxicol Chem.* 1996; 15:181–193.
39. Cabot A, Smith RK, Yin Y, Zheng H, Reinhard BrM, Liu H, Alivisatos AP. Sulfidation of Cadmium at the Nanoscale. *ACS Nano.* 2008; 2:1452–1458. [PubMed: 19206314]
40. Levard C, Reinsch BC, Michel FM, Oumahi C, Lowry GV, Brown GE. Sulfidation Processes of PVP-Coated Silver Nanoparticles in Aqueous Solution: Impact on Dissolution Rate. *Environ Sci Technol.* 2011; 45:5260–5266. [PubMed: 21598969]
41. Liu J, Pennell KG, Hurt RH. Kinetics and Mechanisms of Nanosilver Oxysulfidation. *Environ Sci Technol.* 2011; 45:7345–7353. [PubMed: 21770469]
42. Kim B, Park CS, Murayama M, Hochella MF. Discovery and Characterization of Silver Sulfide Nanoparticles in Final Sewage Sludge Products. *Environ Sci Technol.* 2010; 44:7509–7514. [PubMed: 20839838]
43. Wiesner MR, Lowry GV, Casman E, Bertsch PM, Matson CW, Di Giulio RT, Liu J, Hochella MF. Meditations on the Ubiquity and Mutability of Nano-Sized Materials in the Environment. *ACS Nano.* 2011; 5:8466–8470. [PubMed: 22103257]
44. Zhu H, Wang J, Wu D. Fast Synthesis, Formation Mechanism, and Control of Shell Thickness of CuS Hollow Spheres. *Inorg Chem.* 2009; 48:7099–7104. [PubMed: 19585979]
45. Jiao S, Xu L, Jiang K, Xu D. Well-Defined Non-Spherical Copper Sulfide Mesocages with Single-Crystalline Shells by Shape-Controlled Cu₂O Crystal Templating. *Adv Mater.* 2006; 18:1174–1177.
46. Liu J, Sonshine DA, Shervani S, Hurt RH. Controlled Release of Biologically Active Silver from Nanosilver Surfaces. *ACS Nano.* 2010; 4:6903–6913. [PubMed: 20968290]
47. Reinsch BC, Levard C, Li Z, Ma R, Wise A, Gregory KB, Brown GE, Lowry GV. Sulfidation of Silver Nanoparticles Decreases Escherichia Coli Growth Inhibition. *Environ Sci Technol.* 2012; 46:6992–7000. [PubMed: 22296331]
48. MacCuspie R. Colloidal Stability of Silver Nanoparticles in Biologically Relevant Conditions. *J Nanopart Res.* 2011; 13:2893–2908.
49. Liu J, Hurt RH. Ion Release Kinetics and Particle Persistence in Aqueous Nano-Silver Colloids. *Environ Sci Technol.* 2010; 44:2169–2175. [PubMed: 20175529]
50. Akaighe N, MacCuspie RI, Navarro DA, Aga DS, Banerjee S, Sohn M, Sharma VK. Humic Acid-Induced Silver Nanoparticle Formation under Environmentally Relevant Conditions. *Environ Sci Technol.* 2011; 45:3895–3901. [PubMed: 21456573]
51. Pietruska JR, Liu X, Smith A, McNeil K, Weston P, Zhitkovich A, Hurt R, Kane AB. Bioavailability, Intracellular Mobilization of Nickel, and Hif-1 α Activation in Human Lung Epithelial Cells Exposed to Metallic Nickel and Nickel Oxide Nanoparticles. *Toxicol Sci.* 2011; 124:138–148. [PubMed: 21828359]

52. Yang X, Gondikas AP, Marinakos SM, Auffan M, Liu J, Hsu-Kim H, Meyer JN. Mechanism of Silver Nanoparticle Toxicity is Dependent on Dissolved Silver and Surface Coating in *Caenorhabditis Elegans*. *Environ Sci Technol*. 2011; 46:1119–1127. [PubMed: 22148238]
53. Li X, Lenhart JJ, Walker HW. Dissolution-Accompanied Aggregation Kinetics of Silver Nanoparticles. *Langmuir*. 2010; 26:16690–16698. [PubMed: 20879768]
54. Ho CM, Yau SKW, Lok CN, So MH, Che CM. Oxidative Dissolution of Silver Nanoparticles by Biologically Relevant Oxidants: A Kinetic and Mechanistic Study. *Chem –Asian J*. 2010; 5:285–293. [PubMed: 20063340]
55. Ho CM, Wong CK, Yau SKW, Lok CN, Che CM. Oxidative Dissolution of Silver Nanoparticles by Dioxide: A Kinetic and Mechanistic Study. *Chem –Asian J*. 2011; 6:2506–2511. [PubMed: 21608134]
56. Hirsch MP. Toxicity of Silver Sulfide-Spiked Sediments to the Freshwater Amphipod (*Hyaella Azteca*). *Environ Toxicol Chem*. 1998; 17:601–604.
57. Besser JM, Ingersoll CG, Giesty JP. Effects of Spatial and Temporal Variation of Acid-Volatile Sulfide on the Bioavailability of Copper and Zinc in Freshwater Sediments. *Environ Toxicol Chem*. 1996; 15:286–293.
58. Di Toro DM, Mahony JD, Hansen DJ, Scott KJ, Hicks MB, Mayr SM, Redmond MS. Toxicity of Cadmium in Sediments: The Role of Acid Volatile Sulfide. *Environ Toxicol Chem*. 1990; 9:1487–1502.
59. Bozym RA, Chimienti F, Giblin LJ, Gross GW, Korichneva I, Li Y, Libert S, Maret W, Parviz M, Frederickson CJ, Thompson RB. Free Zinc Ions outside a Narrow Concentration Range are Toxic to a Variety of Cells *In Vitro*. *Exp Biol Med*. 2010; 235:741–750.
60. Zhang L, Yu JC, Yip HY, Li Q, Kwong KW, Xu AW, Wong PK. Ambient Light Reduction Strategy to Synthesize Silver Nanoparticles and Silver-Coated TiO₂ with Enhanced Photocatalytic and Bactericidal Activities. *Langmuir*. 2003; 19:10372–10380.
61. Macomber L, Imlay JA. The Iron-Sulfur Clusters of Dehydratases are Primary Intracellular Targets of Copper Toxicity. *Proc Natl Acad Sci U S A*. 2009
62. Chaturvedi KS, Hung CS, Crowley JR, Stapleton AE, Henderson JP. The Siderophore Yersiniabactin Binds Copper to Protect Pathogens During Infection. *Nat Chem Biol*. 2012; 8:731–736. [PubMed: 22772152]
63. Doğan A, Köseoğlu F, Kılıç E. The Stability Constants of Copper(II) Complexes with Some α -Amino Acids in Dioxan–Water Mixtures. *Anal Biochem*. 2001; 295:237–239. [PubMed: 11488627]
64. Deschamps P, Zerrouk N, Nicolis I, Martens T, Curis E, Charlot MF, Girerd JJ, Prangé T, Bénazeth S, Chaumeil JC, et al. Copper(II)–L-Glutamine Complexation Study in Solid State and in Aqueous Solution. *Inorg Chim Acta*. 2003; 353:22–34.
65. Szecsody JE, Zachara JM, Bruckhart PL. Adsorption-Dissolution Reactions Affecting the Distribution and Stability of CoII in Iron Oxide-Coated Sand. *Environ Sci Technol*. 1994; 28:1706–1716. [PubMed: 22176374]
66. Joshi S, Ghosh I, Pokhrel S, Mädler L, Nau WM. Interactions of Amino Acids and Polypeptides with Metal Oxide Nanoparticles Probed by Fluorescent Indicator Adsorption and Displacement. *ACS Nano*. 2012; 6:5668–5679. [PubMed: 22591378]
67. Oikawa S, Kawanishi S. Site-Specific DNA Damage Induced by NADH in the Presence of Copper(II): Role of Active Oxygen Species†. *Biochemistry*. 1996; 35:4584–4590. [PubMed: 8605209]
68. Folk DS, Franz KJ. A Prochelator Activated by β -Secretase Inhibits A β Aggregation and Suppresses Copper-Induced Reactive Oxygen Species Formation. *J Am Chem Soc*. 2010; 132:4994–4995. [PubMed: 20297791]
69. Mira L, Tereza Fernandez M, Santos M, Rocha R, Helena Florêncio M, Jennings KR. Interactions of Flavonoids with Iron and Copper Ions: A Mechanism for their Antioxidant Activity. *Free Radical Res*. 2002; 36:1199–1208. [PubMed: 12592672]
70. Besser JM, Brumbaugh WG, Ingersoll CG, Ivey CD, Kunz JL, Kemble NE, Schlekot CE, Garman ER. Chronic Toxicity of Nickel-Spiked Freshwater Sediments: Variation in Toxicity among Eight Invertebrate Taxa and Eight Sediments. *Environ Toxicol Chem*. 2013 n/a-n/a.

71. Chakrabarti DJ, Laughlin DE. The Cu-S (Copper-Sulfur) System. *Bull Alloy Phase Diagrams*. 1983; 4:254–271.
72. Luther GW, Theberge SM, Rozan TF, Rickard D, Rowlands CC, Oldroyd A. Aqueous Copper Sulfide Clusters as Intermediates During Copper Sulfide Formation. *Environ Sci Technol*. 2002; 36:394–402. [PubMed: 11871554]
73. Gautam U, Mukherjee B. A Simple Synthesis and Characterization of CuS Nanocrystals. *Bull Mater Sci*. 2006; 29:1–5.
74. Hoffmann MR, Lim BC. Kinetics and Mechanism of the Oxidation of Sulfide by Oxygen: Catalysis by Homogeneous Metal-Phthalocyanine Complexes. *Environ Sci Technol*. 1979; 13:1406–1414.
75. Hollmark HM, Vegelius JR, Kristiansen P, Werme L, Duda LC. Exposure of Oxidized Copper Surfaces to Aqueous Na₂S Solution Studied with Soft X-Ray Spectroscopy. *J Electrochem Soc*. 2011; 158:C1–C5.
76. Raevskaya AE, Stroyuk AL, Kuchmii SY, Kryukov AI. Catalytic Activity of CuS Nanoparticles in Hydrosulfide Ions Air Oxidation. *J Mol Catal A: Chem*. 2004; 212:259–265.
77. Donner E, Howard DL, Jonge MDd, Paterson D, Cheah MH, Naidu R, Lombi E. X-Ray Absorption and Micro X-Ray Fluorescence Spectroscopy Investigation of Copper and Zinc Speciation in Biosolids. *Environ Sci Technol*. 2011; 45:7249–7257. [PubMed: 21793501]
78. Lombi E, Donner E, Tavakkoli E, Turney TW, Naidu R, Miller BW, Scheckel KG. Fate of Zinc Oxide Nanoparticles During Anaerobic Digestion of Wastewater and Post-Treatment Processing of Sewage Sludge. *Environ Sci Technol*. 2012; 46:9089–9096. [PubMed: 22816872]
79. Limbach LK, Wick P, Manser P, Grass RN, Bruinink A, Stark WJ. Exposure of Engineered Nanoparticles to Human Lung Epithelial Cells: Influence of Chemical Composition and Catalytic Activity on Oxidative Stress. *Environ Sci Technol*. 2007; 41:4158–4163. [PubMed: 17612205]
80. Jomova K, Valko M. Advances in Metal-Induced Oxidative Stress and Human Disease. *Toxicology*. 2011; 283:65–87. [PubMed: 21414382]
81. Li M, Zhu L, Lin D. Toxicity of ZnO Nanoparticles to Escherichia Coli: Mechanism and the Influence of Medium Components. *Environ Sci Technol*. 2011; 45:1977–1983. [PubMed: 21280647]
82. VanWinkle, BethA; DMB, KL.; Malecki, JonathanM; Gunter, KarleneK; Evans, IreneM; Elder, Alison; Finkelstein, JacobN; Oberdörster, Günter; Gunter, ThomasE. Nanoparticle (NP) Uptake by Type I Alveolar Epithelial Cells and Their Oxidant Stress Response. *Nanotoxicology*. 2009; 3:307–318. [PubMed: 20563262]

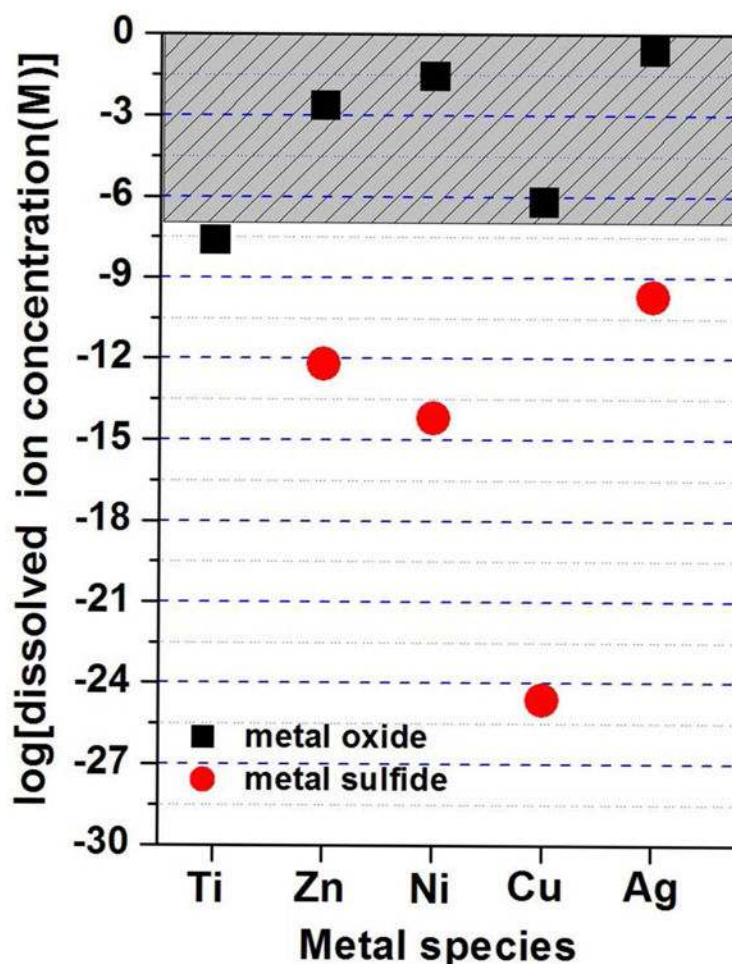


Figure 1.

Equilibrium solubility of the oxide and sulfide forms of common metal-based nanoparticles. The equilibrium dissolved metal ion concentration was estimated using Visual MINTEQ 3.0 using bulk thermodynamic parameters. (See Supporting Information for details) The phases considered were TiO_2 , ZnO , NiO , CuO and Ag_2O and the sulfides ZnS , NiS , CuS and Ag_2S . The incubation conditions for the metal oxide calculations were aqueous solution (pH 7) and 1 mM NaNO_3 as electrolyte, and for metal sulfide ligand-free aqueous solution (pH 7) containing an environmentally relevant total sulfide concentration (1 mM). Please note the calculations ignore any oxidative dissolution. Toxicity studies on free ions typically show adverse biological effects at micromolar doses ($> 0.1 \mu\text{M}$),⁵⁹⁻⁶² which defines the shaded region above. Data points that fall in the shaded region all correspond to cases where nanoparticle toxicity has been attributed to dissolution mechanisms (oxides of Zn, Ni, Cu, Ag), which is possible due to the finite solubility of the oxide phase. TiO_2 solubility in contrast is too low to yield ions above the micromolar range, where ion-induced toxicity is often seen in other systems.

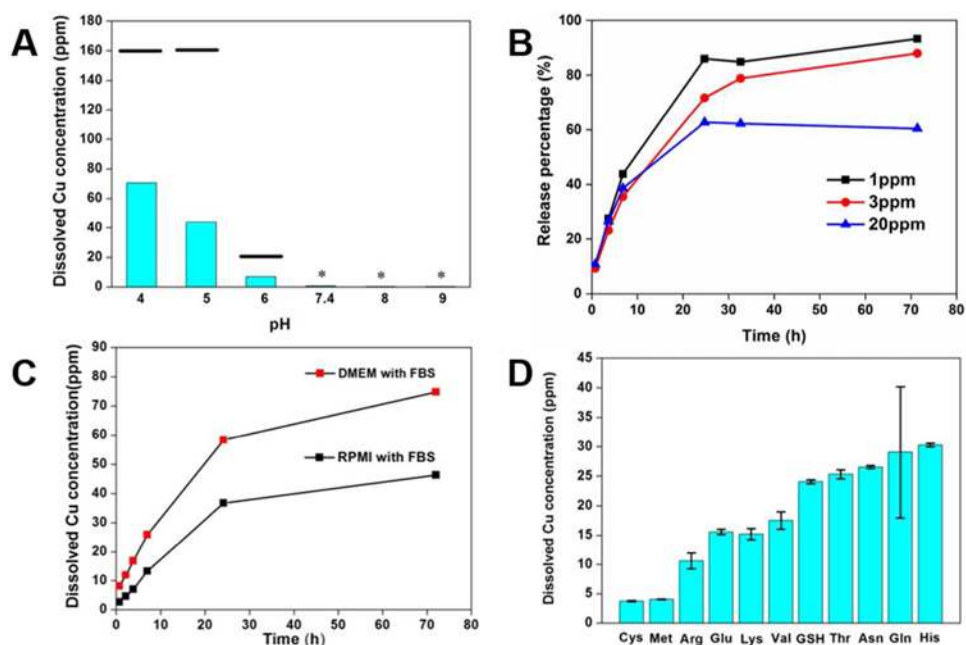


Figure 2. Dissolution behavior of CuO in various fluid media. (A) Soluble copper produced by 24 hr incubation of CuO NPs (initial concentration 200 ppm) as a function of pH (50 mM acetate buffers at pH 4, 5 and 6, PBS buffer at pH 7.4 and 50 mM borate buffers at pH 8 and 9). The black bars indicated the equilibrium concentration in the corresponding pH conditions calculated by Visual MINTEQ 3.0, the stars indicated that both the calculated equilibrium concentration and real dissolved Cu concentration is close to the ICP-AES detection limit. (See Supporting Information for details) (B) Effect of initial CuO NP loading on dissolution kinetics (acetate buffer at pH 4.9) for 3 days expressed as percent of total copper. Over 80% of CuO was dissolved after 30 hours for 1 ppm initial loading of CuO NPs and then dissolved Cu concentration slowly increased. (C) Soluble copper produced by 3-day incubation of CuO NPs (initial concentration 200ppm) in DMEM and RPMI cell culture media supplemented with 10% FBS at pH 7.4. Note the much elevated Cu ion release relative to PBS buffer at pH 7.4 (panel A). (D) Ligand effects on CuO (initial concentration 200 ppm) dissolution using a series of amino acids and the tripeptide glutathione at 2 mM in PBS buffer. Please be noted that the dissolved copper measured is those that pass through the ultrafilters. Therefore, about cysteine, the dissolved copper concentration may be underestimated due to the formation of insoluble precipitate through copper-thiol bond.

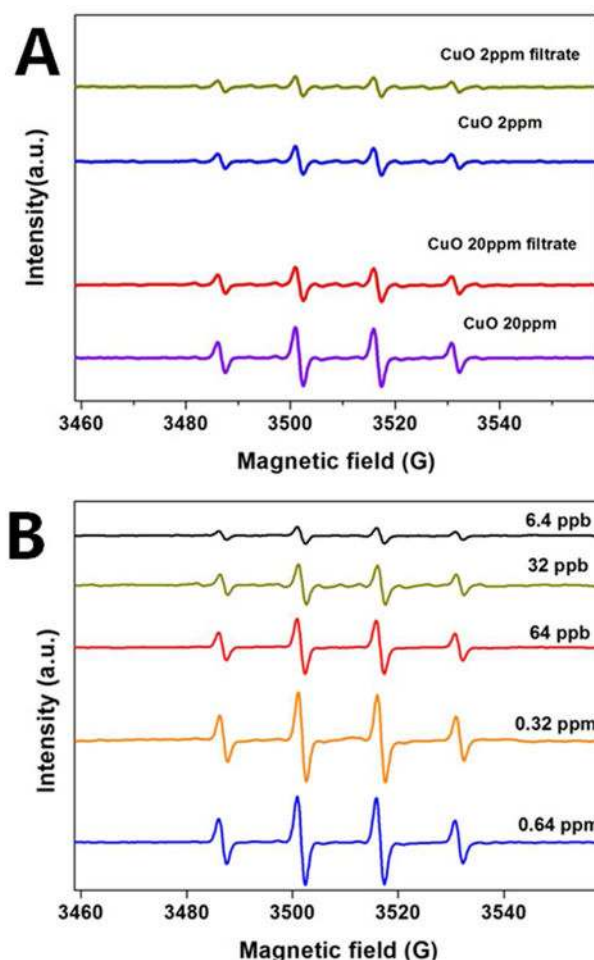


Figure 3. Hydroxyl radical EPR signal (DMPO spin trap) induced by (A) 2 or 20 ppm CuO NPs suspension or its filtrate containing only the soluble forms, (B) free copper ions (CuCl₂) at various concentrations (ppb ng-Cu/g-solution). These experiments used 1 mM hydrogen peroxide and 100 mM DMPO in PBS buffer for 20 min. To isolate the effect of the ion associated with the particles, CuO NPs were incubated for 20 min in PBS buffer then subjected to ultrafiltration, and the filtrate added to 100 mM DMPO and 1 mM hydrogen peroxide in PBS for 20 min before the spectra were obtained (“filtrate” cases in A).

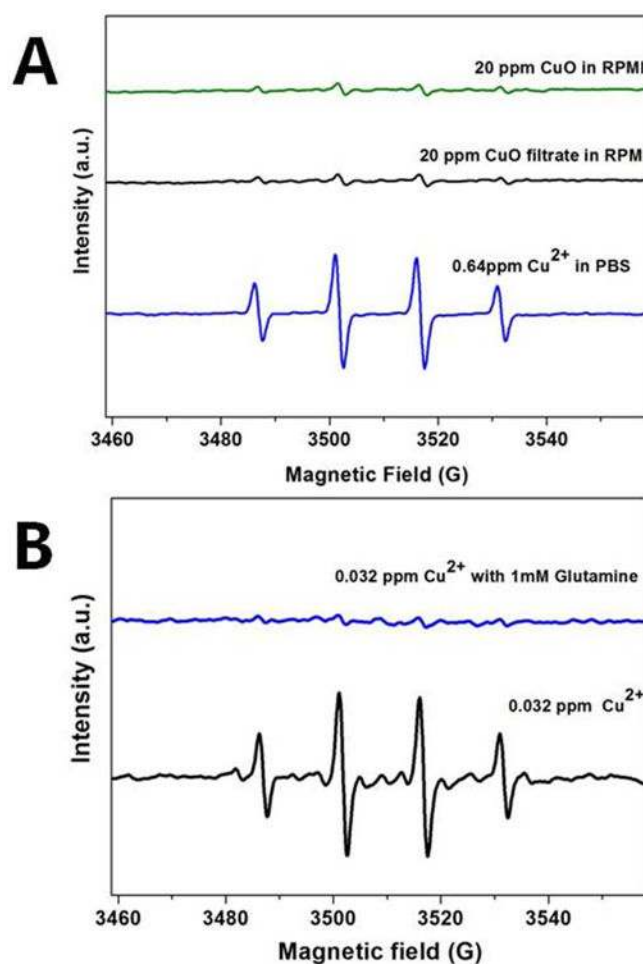


Figure 4. Ligand effects in the ROS activity of CuO-NPs and soluble salts. (A) Comparison of ROS activity of 20 ppm CuO NPs or its filtrate in cell culture media with 0.64 ppm copper ions in PBS buffer. Note that the ion released from 20 ppm CuO-NPs in medium is much greater than the 0.64 ppm free ion concentration (Fig. 2C), but is still less redox active due to ligand binding in medium. (B) ROS activity of 0.032 ppm Cu²⁺ with or without the presence of 1 mM glutamine in PBS buffer. Please be noted that the induced EPR peaks with glutamine were reduced but not eliminated and can increase with longer incubation time according to Figure S3.

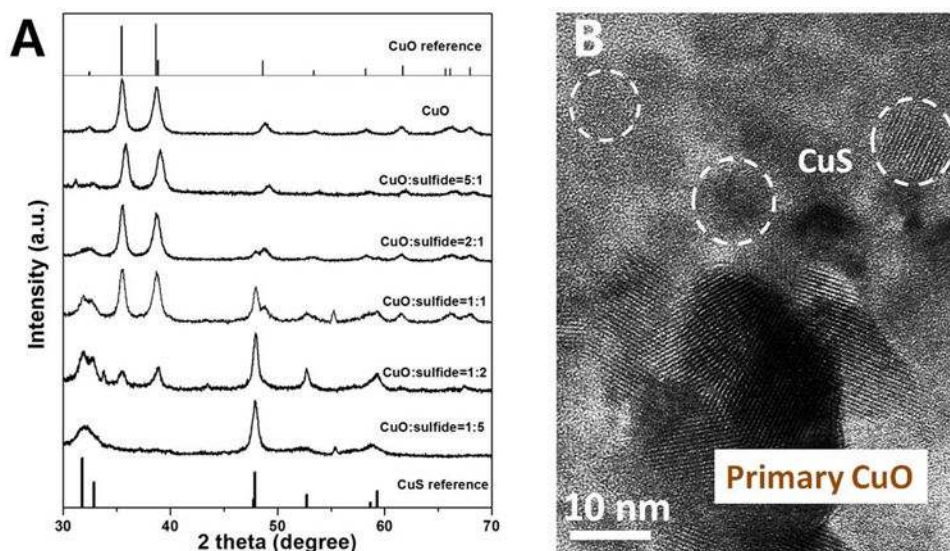


Figure 5. Phases and morphologies of the solid products from reaction of CuO NPs with soluble HS^- . (A) XRD patterns of sulfidated CuO nanoparticles generated from initial Cu/S ratios that vary from 0.2 to 5. CuO (tenorite) and CuS (covellite) reference is presented for comparison. Please note the CuO/CuS peak intensity ratio can't be used to calculate the percentage of CuS produced, but it can show a general trend that CuS produced increase with decreasing CuO to bisulfide ratio. (B) HRTEM image of sulfidated CuO nanoparticles (generated from 2.5 mM of CuO NPs incubated in 5mM Na_2S solution for one day), corresponding to a CuO/bisulfide molar ratio of 1:2. The images show the formation of small secondary particles with size 5 to 10 nm, and showing lattice fringes indicating the presence of at least some crystalline products.

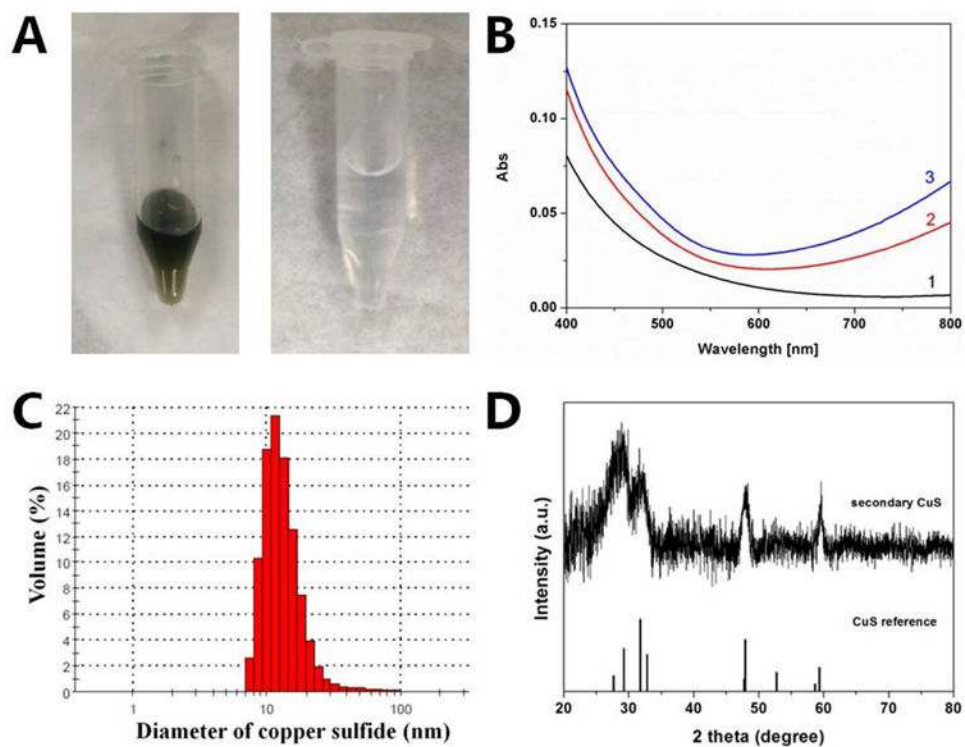
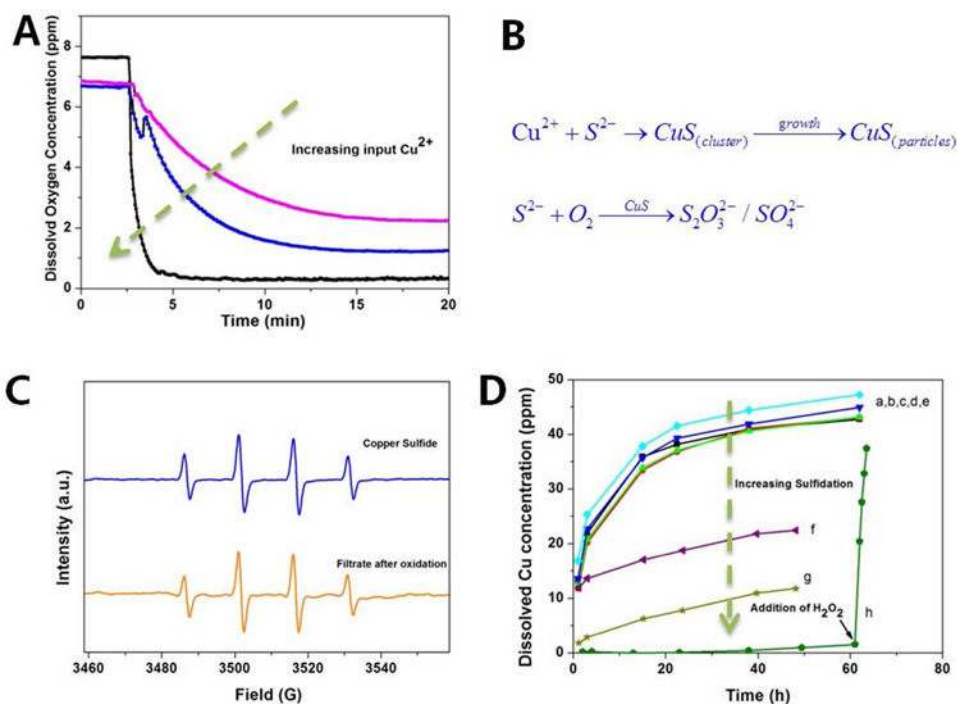


Figure 6. (A) Optical images of concentrated secondary CuS particles through 200 nm filter (left) and the filtrate after CuO NPs suspension in NaOH solution through 200 nm filter (right). (B) UV-vis spectra shows formation of CuS nanoparticles. Curves 1,2,3 correspond to aging for 0, 1, 3 hours, respectively (C) The size distribution of secondary CuS determined by DLS. The original mean size of CuO nanoparticles is 50 nm. (D) XRD pattern confirms the formation of CuS. In these experiments, Na_2S and CuO NPs were incubated at a molar ratio of 2:1.

**Figure 7.**

Properties of sulfidated CuO NPs and implications for toxicity. (A,B) CuS clusters and nanoparticles serve as catalysts for bisulfide oxidation. Reaction tracked through depletion of dissolved oxygen upon addition of copper ions to excess Na_2S solution. Pink, blue and black curves correspond to addition of 0.1, 1 or 2 mM copper ion. (C) Hydroxyl radical EPR signal induced by a 0.1 mM CuS suspension and its particle-free filtrate after hydrogen peroxide treatment. Despite low solubility, CuS shows redox activity associated with soluble species. (D) Dissolution behavior of CuS and a series of partially sulfidated CuO NPs at pH 4 acetate buffer. The sulfidation was carried out using 2.5mM CuO at the initial S/Cu ratios from 0.2 to 5. (a, b, c, d, e represents the dissolution of CuO, sulfidated CuO with S/Cu at 0.1, 0.2, 0.5, 1, which has little effect on CuO dissolution; f, g represents the dissolution behavior of sulfidated CuO with S/Cu at 2, 5 respectively, which can slow the dissolution rate.) The pure CuS solid was prepared through precipitation of Cu^{2+} and bisulfide in stoichiometric mixture followed by washing and resuspension. To understand the redox behavior in (C) the oxidative-dissolution of CuS was investigated by adding H_2O_2 solution in equimolar proportion to CuS.

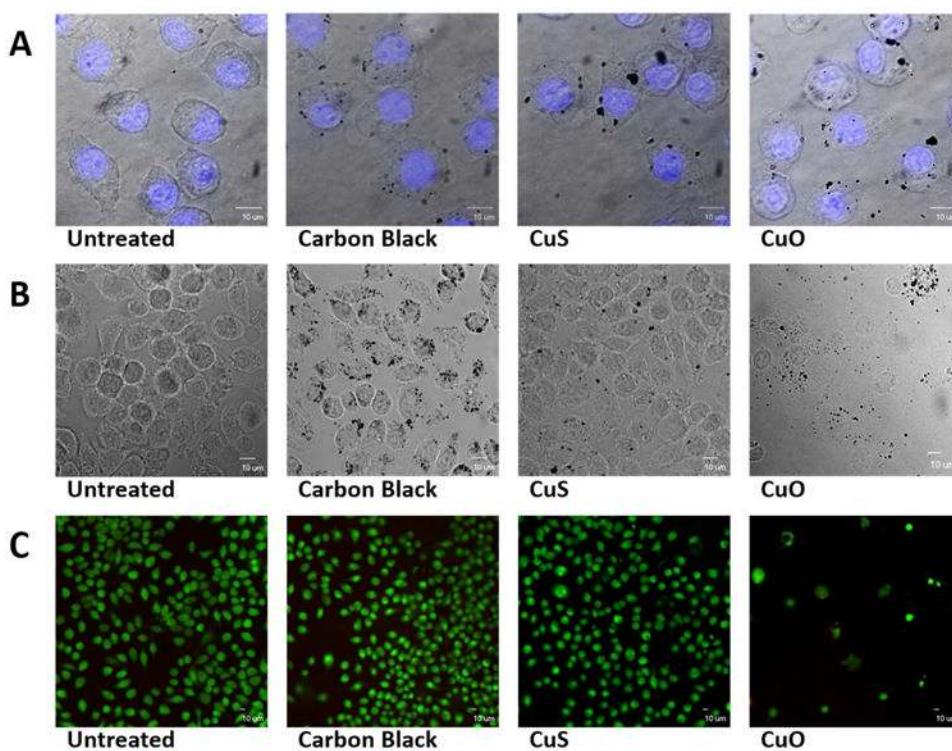


Figure 8. Target cell uptake and toxicity of carbon black, CuS, and CuO NPs. (A) Confocal images of murine macrophages after exposure to 5 ppm of test particles for 3 hours; nuclei were visualized (blue fluorescence) using 4'6-diamidino-2-phenylindole (DAPI). (B) Brightfield microscopic images of murine macrophages 24 hours after exposure to 5 ppm of test nanoparticles. (C) Viability of target cells 24 hours after exposure to 5 ppm of test nanoparticles. Viable cells show green cytoplasmic fluorescence (Syto 10/ethidium homodimer assay).

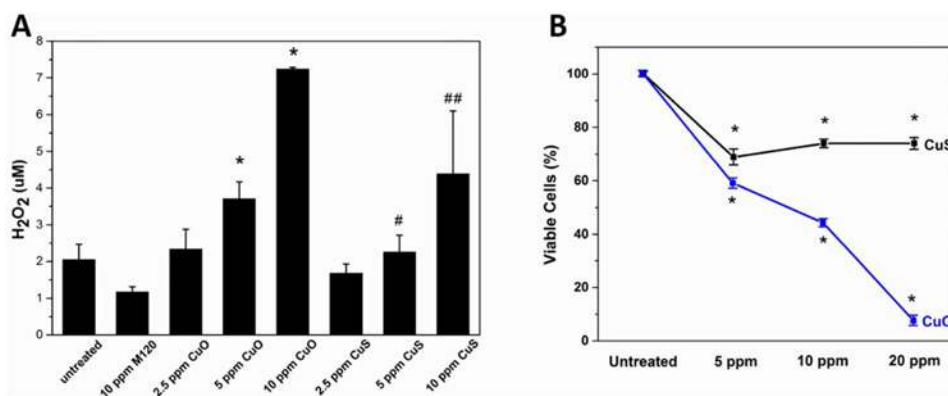


Figure 9.

(A) Generation of H₂O₂ by murine macrophages exposed to carbon black, CuO and CuS NPs. Detection of H₂O₂ production in macrophages exposed to 2.5 ppm, 5 ppm, or 10 ppm of CuO, CuS or M120 (carbon black) as determined using the Amplex Red assay 20 minutes after exposure. Cells exposed to higher concentrations of CuO demonstrate significantly increased generation of H₂O₂ compared to untreated controls or CuS-exposed cells. **p* < 0.05 compared to control; #*p* < 0.05 compared to 5 ppm CuO; ##*p* < 0.05 compared to 10 ppm CuO. (B) Viability of murine macrophages after exposure to CuS NPs or CuO NPs for 48 hours. DNA content relative to untreated control cells was determined using Pico Green fluorescence as a surrogate for cell number. Differences in viability of cells exposed to each dose of CuS or CuO NPs relative to untreated controls was statistically significant after 48 hours. **p* < 0.05 compared to control.

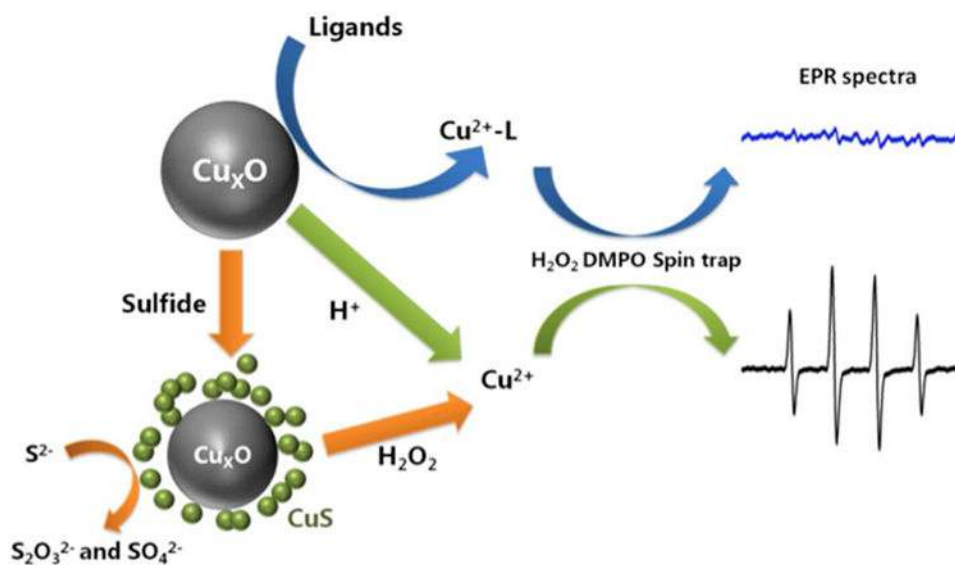


Figure 10. Summary of chemical transformations and redox behaviors of Cu-based nanoparticles in biological and environmental media.